ELSEVIER

Ceramics International 30 (2004) 2251–2257

CERAMICS INTERNATIONAL

www.elsevier.com/locate/ceramint

Point load-induced fracture behavior in zirconia plasma spray coating

Yoshio Akimune [a,*], Kazuo Matsuo [a], Satoshi Sodeoka [a], Tatsuo Sugiyama [a], Satoshi Shimizu [b]

[a] *National Institute of Advanced Industrial Science and Technology, 1-1-1 Umezono, Tsukuba, Ibaraki-Prefecture 305-8568, Japan*
[b] *Nissan Arc, Ltd, 1, Natsushima-cho, Yokosuka, Kanagawa-Prefecture 237-0061, Japan*

Received 30 May 2003; received in revised form 3 November 2003; accepted 30 December 2003
Available online 17 April 2004

Abstract

Heat-resistant coatings prepared by two different spraying methods: atmospheric pressure plasma spraying (APS) and high-pressure plasma spraying (HPPS), were tested using tungsten carbide indenters of different diameters, for the purpose of proposing the best suited method of indentation testing. It was found that with the APS method, the indentation load–depth curve gave the indentation depth and the residual depth smaller than and the yield stress greater than those with the HPPS. On the basis of fracture morphology in the cross-section, it has been conjectured that the APS coating has greater elastic modulus than the HPPS coating, and exhibits high strength exceeding debonding force between bond coat and top coat.

Keywords: Indentation; Plasma spray coating; Hertz cone crack; Elastic–plastic response debonding

1. Objective

The heat-resistant coating technology is used for the protective surface coating of the metal blades in the generator gas turbine, which is the mainstay equipment of the thermal power generation. As the fuel species shift to heavy oil and coal in the days ahead, it is of concern that problems of combustion residuals and utilization under corrosive atmosphere may arise. The use of turbine blades with protective coating involves debonding of coating triggered by point load-induced fractures through bombardments with combustion residuals. This may lead to substrate damages and must be resolved immediately.

For the evaluation of mechanical properties of ceramic protective coating for the turbine blade, a number of reports are available in regard to damage morphology evaluation based on the load–stress curves of coating induced by point load impact, such as Pajares et al. [1,2], Wuttiphan et al. [3], Swain and Menčık [4], Lee et al. [5]. These studies are derived from the theoretical analysis works by Hertz [6], Timoshenko and Goodier [7], and Johnson [8]. Papers on ceramics damage are reviewed by Lawn [9].

The present study aims at proposing an optimum method for indentation tests to detect damages in heat-resistant coating prepared by either of two spray techniques: atmospheric plasma spraying (APS) and high-pressure plasma spraying (HPPS). In the experiment, specimens were prepared by covering Inconel 600 substrate with a bond coat and either of two zirconia spray coats, and indented with spherical indenters through a quasi-static method, subsequently examining the fracture and debond behaviors of the coats.

2. Experimental methods

2.1. Sprayed specimen

The specimen consisted of a substrate of Inconel 600, a spray coat of zirconia stabilized with 8 mass% (METECO 204NS-G) and an intermediate bond coat of NiCoCrAlY (AMDRY-1). The substrate surface was polished with #70 alumina to make the roughness to Ra = 5 μm, and cleaned by reverse sputtering at 1073 K immediately before adding

* Corresponding author.
E-mail address: y-akimune@aist.go.jp (Y. Akimune).

0272-8842/$30.00 © 2004 Elsevier Ltd and Techna S.r.l. All rights reserved.
doi:10.1016/j.ceramint.2003.12.008

Nomenclature

a	indent impression radius
E_s	Young's modulus of substrate
E_i	Young's modulus of indenter
h	indentation depth
h_y	impression depth
K_e	composite Young's modulus
P	pressure
P_m	indentation pressure
p_0	contact pressure
P_y	yield stress
R	indenter diameter
ν_s	Young's modulus of substrate
ν_i	Young's modulus of indenter

bond coat. The substrate temperature was not measured after that. The top coat was provided either by APS or by HPPS using 200 kPa Argon to make up a zirconia coat of 200 μm thickness. Spray parameters are listed in Table 1. The construction of plasma spray system is described in the literature [10].

2.2. Testing methods

2.2.1. Microindentation test [11]

The coated film was indented with a spherical indenter of tungsten carbide (WC) at a specified speed ($v = 1.67$ μm/s), with load (P) and impression depth (h) measured after having unloaded. With an indenting equipment consisting of an indenter mounted on a strength testing machine (Instron #5867) the impression depth and the load–depth curve were recorded at the room temperature, 0.05 mm/min crosshead speed and 1 kN load (Fig. 1). Then, the data were converted into the load–stress curve by using a theoretical equation shown in the later part, $P_m \propto (h/R)^{0.5}$ to calculate the yield stress. Loading and unloading were carried out at the same speed, and the depth–unload curve was measured three times. The maximum load was set to 1 kN. At the peak load, the crosshead of the testing machine was reversed, with the load retained for 1 s or so, owing to the mechanical play.

2.2.2. Preparation of specimen

The test-piece was prepared by cutting into approximately 15 mm × 15 mm × 3 mm plate and the sprayed surface was polished to Ra = 0.2 μm with abrasive agent (Buehler, colloidal silica 0.06 μm). The residual thickness of spray layer was 95 and 85 μm for APS and HPPS, respectively, while the bond coat was about 115 μm in thickness.

2.2.3. Indent impression observation

After the indentation test, the impression on the surface was observed by the optical microscopy. The specimen was cut in the vicinity of the indent impression, embedded in epoxy resin with the sectional face upward, and polished to the center of the impression using abrasive agent (Buehler, colloidal silica 0.06 μm), to be observed under an optical microscope in the bright field.

2.2.4. Analysis of static indentation behavior

2.2.4.1. Load calculation [6–8]. The pressure caused by the indentation of a blunt indenter is given by the equation:

$$\frac{P}{\pi a^2} = \left(\frac{3E}{4\pi k}\right)\left(\frac{a}{R}\right) = p_0 \quad (1)$$

which was derived from Hertz's theory of elasticity, $a^3 = 4kPR/3E$, where a is the indent impression radius, R is the indenter diameter, and $k = 9/16[(1-\nu_s^2) + (1-\nu_i^2)E_s/E_i]$,

Table 1
Plasma spraying condition

	Bond coat	Top coat	
		Atmospheric plasma spraying	High-pressure plasma spraying
Materials	NiCoCrAlY (AMDRY365-1)	8 mass% Y_2O_3 stabilized ZrO_2 (METCO204NS-G)	8 mass% Y_2O_3 stabilized ZrO_2 (METCO204NS-G)
Particle size	45–53 μm	11–106 μm	11–106 μm
Substrate roughness	Ra: 5 μm		
Coating temperature	1073 K pre-heating	1073 K pre-heating	1073 K pre-heating
Type of plasma torch	Sulzer Meteco F4VB	Sulzer Meteco F4VB	Sulzer Meteco F4VB
Atmosphere and flow rate	Ar: 50 l/min	Air	Ar: 50 l/min
Anode nozzle internal diameter	7 mm	7 mm	7 mm
Type of injection	Internal	Internal	Internal
Injector internal diameter	3.0 mm	1.5 mm	1.5 mm
Pressure	10 kPa	Air	200 kPa
Spray distance	300 mm	100 mm	10 mm
Gas flow	Ar: 50 l/min; H_2: 9 l/min	Ar: 42 l/min; H_2: 10 l/min	Ar: 50 l/min; H_2: 5 l/min; He: 10 l/min
Powder feed	0.025 kg/min	0.0048 kg/min	0.0052 kg/min

Fig. 1. An overall view of quasi-static indentation testing system.

where E_s and E_i are Young's modulus, and ν_s and ν_i are Poisson's ratio, of substrate and indenter, respectively.

If the impression depth h is used, the relation is written as $R^2 = a^2 + (R-h)^2$, which may be approximated with $(a/R)^2 = h/R$, if $R \gg h$. The relationship of p_0 to $(h/R)^{0.5}$ will be plotted subsequently.

2.2.4.2. Composite Young's modulus. The composite Young's modulus was calculated from expressions (2) and (3) with slope (K_e) and yielding point (yield stress: P_y and impression depth: h_y), using a graph plotting indent load on the ordinate and 3/2 power of impression depth on the abscissa.

$P = K_e h^{3/2}$ (relation of pressure to impression depth)

$$K_e = \frac{4}{3}(RE^*)^{1/2} \text{ (composite Young's modulus)} \quad (2)$$

$$\frac{1}{E^*} = \frac{(1-\nu_s^2)}{E_s} + \frac{(1-\nu_i^2)}{E_i} \quad (3)$$

$$P_m = \frac{P_y}{\pi R h} \quad (4)$$

where E_i and E_s are the Young's modulus of indenter (WC: 534 GPa) and substrate (Inconel: 200 GPa), ν_i and ν_s are the Poisson's ratio of indenter (WC: 0.28) and substrate (Inconel: 0.3), P_m is the indentation pressure, and P_y is the yield stress.

3. Results and discussion

3.1. Quasi-static indentation test

3.1.1. Continued load/unload test

Indentation load–depth curves with APS and HPPS specimens following an indentation are shown in Fig. 2a and b, respectively, and stress–strain curves at indentation obtained by the indentation method are in Fig. 3a and b. In the former curves, it was demonstrated that the smaller the indenter size was, the greater the impression depth became, and the impression depth with HPPS specimen was greater than that with APS. In case of HPPS specimens, the slope of unloading curve was steeper, and the impression depth was close to the residual depth. Non linearity of the stress–strain curve with 1 mm Ø spherical indenter in Fig. 2a and b seems to be attributable to the effects of indent location on the coat, where bond coat and top coat have uneven thickness. For both APS and HPPS specimens, the results with 1 mm Ø indenter should be handled with care. In case of 2 and 4 mm Ø indenters, the increment in strain fails to conform to that in stress, suggesting the occurrence of plastic deformation.

The yield stress (P_y), represented by an inflection point from the initial slope tended to decrease with the increase in the indenter size (Fig. 3a and b). Since a similar trend was seen in the substrate, Inconel 600, the difference may be attributed to the elastic–plastic response of spray coat depending upon the plastic deformation of substrate, or to the difference in fracture morphology of coat. While HPPS specimens shows smaller yield stress than that of APS, the latter presented low-profile behaviors subsequently, indicating ready occurrence of fracture in spray coat.

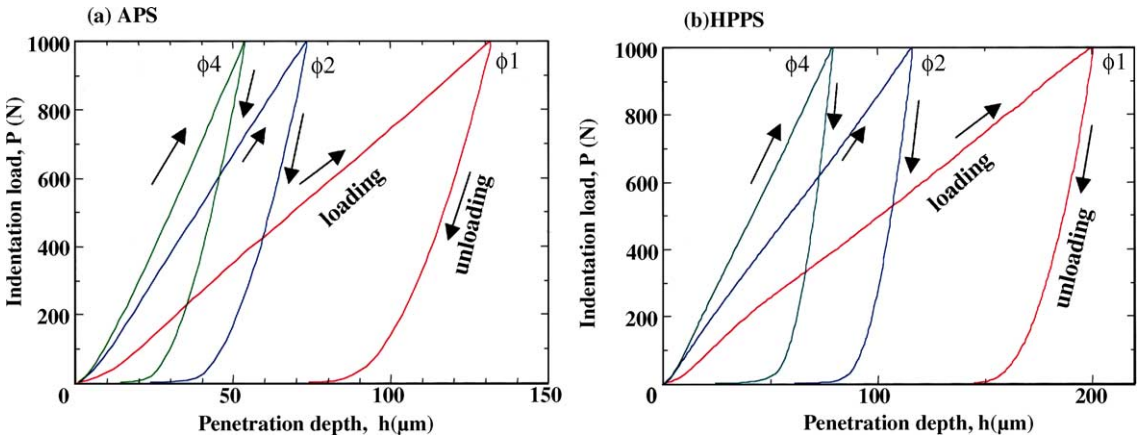

Fig. 2. Indent–unload curve with spherical indenter.

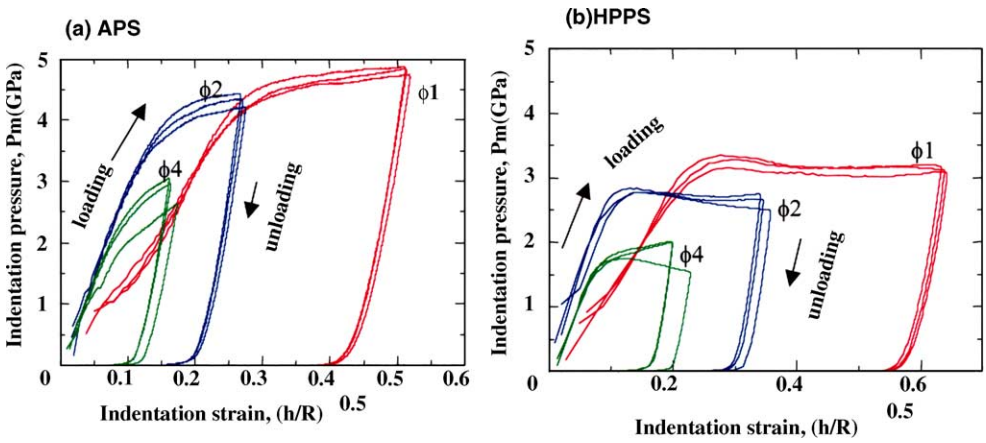

Fig. 3. Stress–strain curve for the indentation testing.

3.1.2. Surface observation

Results of indent impression surface observation with APS and HPPS specimens after the indentation and unloading are shown in Fig. 4a and b, respectively. The APS specimen presented a indent impression on the surface, while in case of HPPS the indent impression was surrounded with a circular depression. Combined with the post-yield behavior after the indentation, this suggests that the spray coat is subjected to a force exceeding the yield stress of materials in the course of indentation loading–unloading test to cause fine cracks, which increase the apparent indenter radius. The results seem to be in line with the flat post-yield behavior in Fig. 3 due to decreased contact pressure.

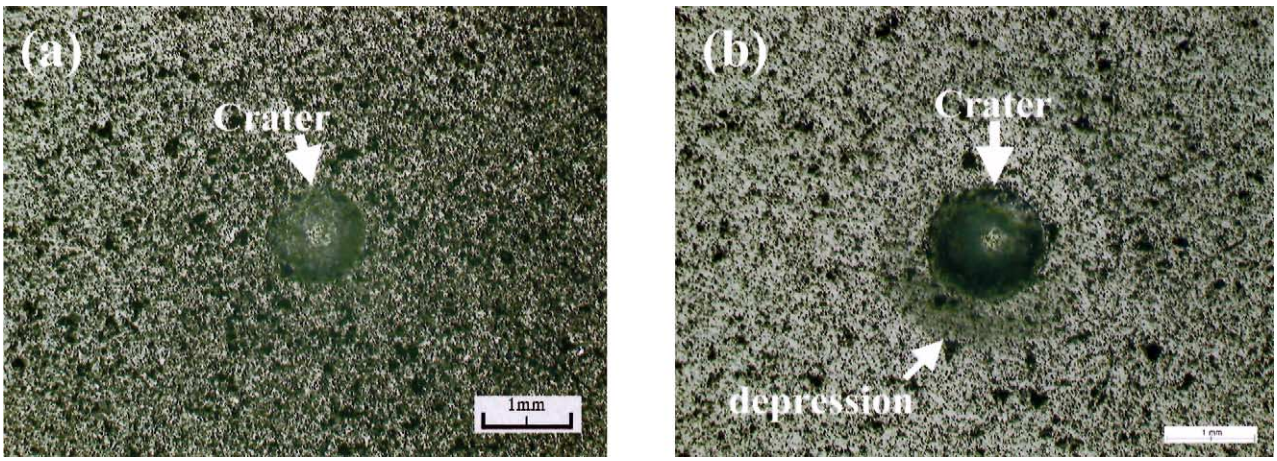

Fig. 4. Indent impression. (a) Atmospheric plasma spraying with 95 μm, indenter 4 mm Ø. (b) High-pressure plasma spraying with 85 μm, indenter 4 mm Ø.

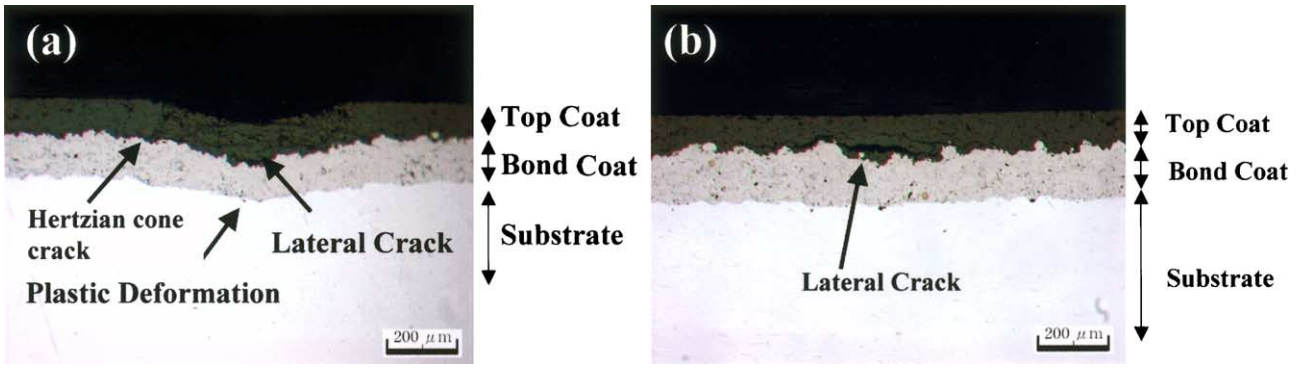

Fig. 5. Cross-section of indent impression. (a) Atmospheric plasma spraying, indenter 1 mm Ø. (b) Atmospheric plasma spraying, indenter 4 mm Ø.

3.1.3. Cross-sectional observation

The results of cross-sectional observation for indent impression with different specimens and indenter diameters are shown in Figs. 5 and 6. The difference in effects of indenter size is exaggerated depending upon the spray method. In case of APS specimens (Fig. 5), 1 mm Ø indenter caused the fracture morphology of Hertz cone crack, rather than debonding, and when unloaded, the direction of stress changed to induce debonding at the top coat/bond coat interface, too [12]. In the case of 4 mm Ø indenter, lateral crack was significant. The smaller the indenter size was, the higher the pressure grew (Fig. 3a), causing more pronounced plastic deformation [1,2] of substrate immediately below the indent impression. With 1 mm Ø indenter, the plastic deformation was proportional to the damage area, but in case of 4 mm Ø, the area of plastic deformation was minor. Based on the morphology of fracture and debonding, it may be conjectured that the APS gives a hard coat, presenting initially elastic behavior with Hertzian cracks, which is gradually followed by elastic–plastic response behavior. For this reason, lateral cracks and debonding are seen at the interface between the bond coat and the substrate which are attributable to changes in stress field at the time of unloading. That is, debonding occurred at the top coat/bond coat interface where the bonding force was considered weakest, as the loading released the elastic stress energy accumulated at the bond coat and the substrate in the form of repulsive force, with stress acting vertically to the bond coat [12].

With the HPPS specimens (Fig. 6), the plastic deformation of substrate and Hertzian cone cracks behaved in similar way as in the APS specimens, for the case of 1 and 4 mm Ø indenter. The lateral cracks within the top coat were more prominent than the debonding at top coat/bond coat interface, as seen in the APS specimen at the time of unloading. This may be attributed to the strength of top coat materials, inferior to the bonding strength of interface. With the 4 mm Ø indenter, deformation of the substrate is still observed. Hertzian cone crack was also seen and the lateral cracks are extended to a wide area making the coat nearly drop out.

3.2. Calculation of Young's modulus and yield stress

The relationship of indenter diameters to parameters of mechanical property is shown in Figs. 7 and 8. Fig. 7 shows that the composite Young's modulus (K_e in Eq. (2)) was small with 1 mm Ø indenter, while those for 2 and 4 mm Ø indenters were nearly identical. The Young's modulus is a constant specific to materials, and should not change by indenter size. The observed variation may be ascribed to mechanical behaviors such as plastic deformation and cracks immediately below the indenter. These responses require further investigation. In Fig. 8, the yield stress decreases gradually. But the spray methods provide contrasting effects:

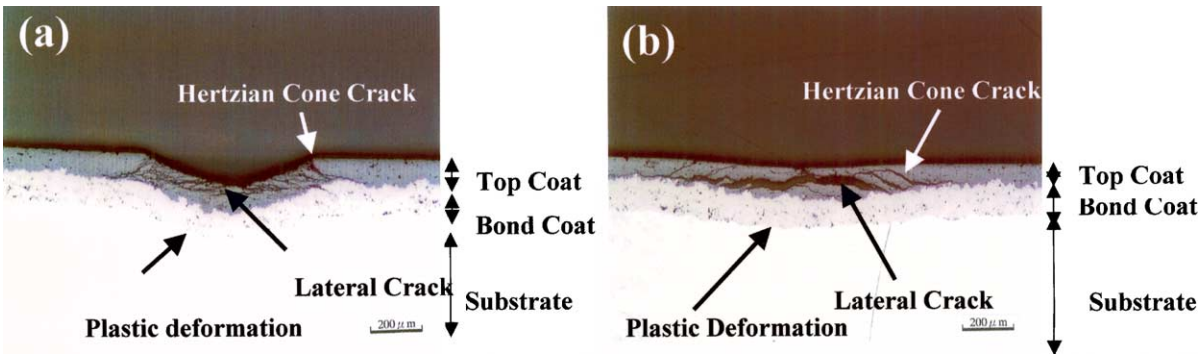

Fig. 6. Cross-section of indent impression. (a) High-pressure plasma spraying, indenter 1 mm Ø. (b) High-pressure plasma spraying, indenter 4 mm Ø.

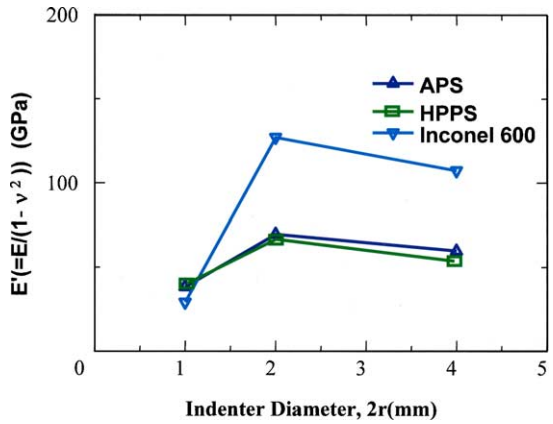

Fig. 7. The relation between composite Young's modulus and indenter diameter.

with the HPPS specimen, the yield stress is low regardless of indenter size, close to that of substrate. This value is reflected in the penetration depth in Fig. 2 and the indentation pressure in Fig. 3, representing the crack generating behavior caused by point load.

3.3. The relationship between P–h curve and fracture morphology for different spray methods

With the APS specimens, the test with 1 mm Ø indenters provided pronounced plastic deformations in the substrate and the bond coat, and the substrate presented elastic–plastic deformations. Hertzian cone crack, which shows elastic response behavior at the very early stage of indent, was observed. When 4 mm Ø indenters were used, the plastic deformation in the substrate and the bond coat was reduced, and the cross-section revealed debonding between top and bond coats. In addition to debonding, a number of cracks were recognized in parallel to the substrate, suggesting the occurrence in the course of unloading. While the plastic deformation area was reduced, lateral cracks were seen at the time of unloading. According to Ref. [4], debonding in the course of loading can be judged on the basis of inclination point in the *P–h* curve. In the present case, however, no inclination point was observed clearly at the time of loading, rather indicating the validity of inferring from the residual depth in the *P–h* curve shown in Fig. 2.

For HPPS specimens, plastic deformation was pronounced in the substrate and the bond coat with 1 mm Ø indenters, while the substrate presented Hertzian cone cracks, porous zones infested with cracks, as well as lateral cracks. When 4 mm Ø indenters were used, the plastic deformation area in the substrate and the bond coat was reduced, but the lateral cracks inferred to have occurred in the course of unloading expanded. These fracture behavior is thought to be related with the residual depth in the *P–h* curve shown in Fig. 2b becomes bigger according to the expanding lateral cracks in the top coating.

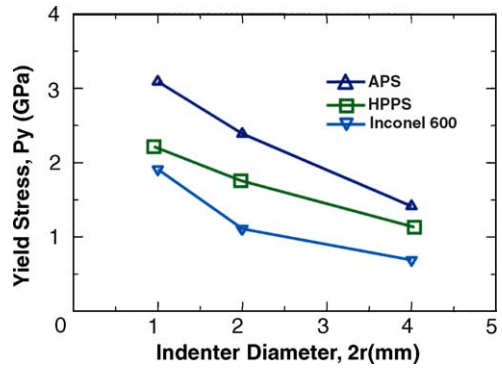

Fig. 8. The relation between yielding stress and indentation diameter.

4. Conclusion

In the present study, the indentation test using tungsten carbide indenters of different diameters was carried out, for the purpose of proposing an optimum method of indentation testing, using two types of heat-resistant coating prepared through different plasma spray methods: APS and HPPS.

The APS coat was found to present more elastic behavior than the HPPS coat, and to be strong enough to surpass the debonding force at top coat/bond coat interface. The results seemed to be reflected in smaller penetration depth and residual depth in the load–strain curves at the time of indentation and higher yield stress.

Acknowledgements

This work was carried out by the authors and members of the Nano-coating Research Group as a part of the Nanostructure Coating Technology Project in the Nanotechnology Program (Nanomaterials Process Technology) under the Industrial Science and Technology R&D Program of the Ministry of Economy, Trade and Industry (METI) and entrusted by the New Energy and Industrial Technology Development Organization (NEDO).

References

[1] A. Pajares, L. Wei, B.R. Lawn, Contact damage in plasma-sprayed alumina-based coatings, J. Am. Ceram. Soc. 79 (7) (1996) 1907–1914.
[2] A. Pajares, L. Wei, B.R. Lawn, N.P. Padture, C.C. Berndt, Mechanical characterization of plasma sprayed ceramic coatings on metal substrates by contact testing, Mater. Sci. Eng. A208 (1996) 158–165.
[3] S. Wuttiphan, A. Pajares, B. Lawn, C.C. Berndt, Effect of substrate and bond coat on contact damage in zirconia-based plasma-sprayed coatings, Thin Solid Films 293 (1997) 251–260.
[4] M.V. Swain, J. Menčík, Mechanical property characterization of thin films using spherical tipped indenters, Thin Solid Films 253 (1994) 204–211.

[5] K.-S. Lee, S. Wuttiphan, X.-Z. Hu, S.-K. Lee, B.R. Lawn, Contact-induced transverse fractures in brittle layers on soft substrate: a study on silicon nitride bilayers, J. Am. Ceram. Soc. 81 (3) (1988) 571–580.
[6] H.R. Hertz, Hert's Miscellaneous Papers, Macmillan, London, 1896 (Chapters 5 and 6).
[7] S.P. Timoshenko, J.N. Goodier, Theory of Elasticity, 3rd ed., McGraw-Hill Book Company, pp. 409–415.
[8] K.L. Johnson, Contact Mechanics, Cambridge University Press, pp. 84–106.
[9] B.R. Lawn, Indentation of ceramics with spheres: a century after Hertz, J. Am. Ceram. Soc. 81 (8) (1998) 1977–1994.
[10] S. Sodeoka, M. Suzuki, K. Ueno, Effects of high-pressure plasma spraying for yttria-stabilized zirconia coating, J. Therm. Spray Technol. 5 (3) (1996) 277–282.
[11] S. Shimizu, Ph.D. Dissertation (in Japanese), Toyoshashi Institute of Technology, 2001.
[12] D.B. Marshall, B.R. Lawn, A.G. Evans, Elastic/plastic indentation damage in ceramics—the lateral crack system, J. Am. Ceram. Soc. 65 (11) (1982) 561–566.